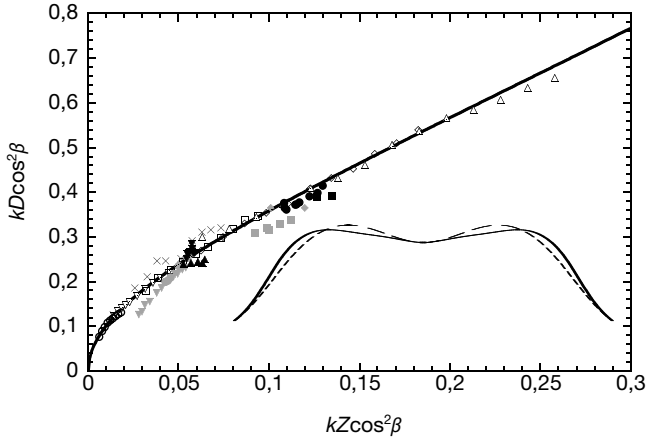

Figure 4 Distance between the dominant d-cones and the centre with various α and d values. k is half the mean curvature at the plate centre when $Z = 0$. Crosses, numerics; the other symbols are experimental. Open symbols, two-cones regime. Grey symbols, diamond regime. Black symbols, trapezoid regime. Solid line, theoretical prediction from equation (3). Inset curve ($Z = 6$ mm), x cross-section of the plate (solid line); elastic arch (dashed line).

(3)) hold when k is replaced by $k\cos^2\beta$ as is checked in Fig. 4. To lowest order in kZ, the d-cone radius is $R \approx D \approx \cos\beta\sqrt{Z/k}$. If the interaction between the d-cone and the clamped boundary is strong, the d-cone is constrained to move to a new position $\beta \neq 0$, in which the periphery of the d-cone (a circle of radius R) exactly touches the boundary of the plate, $D\cos\beta + R = W/2$. For Z near to Z_c, this condition leads to

$$\beta \approx \pm 4\sqrt{2/3}/kW\sqrt{k(Z - Z_c)} \qquad (4)$$

Here $4\sqrt{2/3}/kW = 3.3$ and $Z_c = 10.9$ mm compare well with the experimental $\beta = 3.1\sqrt{k(Z - Z_c)}$ with $Z_c = 10$ mm.

Now consider the second pair of d-cones. When their peripheries touch the clamped boundaries, $\beta + \theta \approx \pi/2$ so that $Z = Z_t \approx k(W/2/\sin\theta/(1 + \sin\theta))^2 = 15$ mm (with $\theta = 63°$) which is comparable to the experimental $Z_t = 12$ mm. For $Z \geqslant Z_t$ all d-cones have to move along the clamped boundaries. If two of them are constrained to have an angular opening of 2θ, the only possible shape is a trapezoid. Compared to the two-d-cones regime, energy is gained in the diamond, and then the trapezoid regime. These configurations were not observed numerically, probably owing to the discretization. For this reason the numerics overestimates the force in region IV of Fig. 3. At $Z \geqslant 13$ mm the plate becomes cylindrical (pure bending deformations) so that the force jumps to a much smaller value (Fig. 3). This transition is well predicted by the numerics. The energy of the plate is then the same as the elastic arch[13].

The experiment we have performed is typically a controlled version of what happens when a car is bumped. The difference is in the material; in metals the elastic limit is easily exceeded at the d-cones and then at the ridges. The first deformation of a plate is either cylindrical or conical. Most further deformations lead to the formation of pairs of d-cones and to the diamond-shaped deformation we have studied here. The observed shapes are determined by the geometry, and the energy of the plate can be computed using only the energy of the singularities. □

Received 22 February; accepted 24 July 2000.

1. Pogorelov, A. V. *Bendings of Surfaces and Stability of Shells.* (Translations of Mathematical Monographs No. 72, American Mathematical Society, 1988).
2. Witten, T. A. & Li, H. Asymptotic shapes of a fullerene ball. *Europhys. Lett.* **23,** 51–55 (1993).
3. Lobkovsky, A. E., Gentges, S., Li, H., Morse, D. & Witten, T. A. Scaling properties of stretching ridges in a crumpled elastic sheet. *Science* **270,** 1482–1485 (1995).
4. Lobkovsky, A. E. Boundary layer analysis of the ridge singularity in a thin plate. *Phys. Rev. E* **53,** 3750–3759 (1996).
5. Ben Amar, M. & Pomeau, Y. Crumpled paper. *Proc. R. Soc. Lond. A* **453,** 729–755 (1997).
6. Chaïeb, S. & Melo, F. Experimental study of developable cones. *Phys. Rev. Lett.* **80,** 2354–2357 (1998).
7. Cerda, E. & Mahadevan, L. Conical surfaces and crescent singularities in crumpled sheets. *Phys. Rev. Lett.* **80,** 2358–2361 (1998).
8. Cerda, E., Chaïeb, S., Melo, F. & Mahadevan, L. Conical dislocations in crumpling. *Nature* **401,** 46–49 (1999).
9. Chaïeb, S. & Melo, F. Experimental study of crease formation in an axially compressed sheet. *Phys. Rev. E* **56,** 4736–4745 (1997).
10. Pomeau, Y. & Rica, S. Plaques très comprimées. *C.R. Acad. Sci. Paris* **325**, Série IIb, 181–187 (1997).
11. Pauchard, L. & Rica, S. Contact and compression of elastic spherical shells. *Phil. Mag. B* **78,** 225–233 (1998).
12. Pippard, A. B. The elastic arch and its modes of instability. *Eur. J. Phys.* **11,** 359–365 (1990).
13. Patrício, P., Adda-Bedia, M. & Ben Amar, M. An *elastica* problem: Instabilities of an elastic arch. *Physica D* **124,** 181–187 (1998).
14. Landau, L. D. & Lifshitz, E. M. *Theory of Elasticity* (Pergamon, Oxford, 1986).
15. Patrício, P. & Krauth, W. Numerical solutions of the Von Karman equations for a thin plate. *Int. J. Mod. Phys. C* **8,** 427–434 (1997).

Acknowledgements

We thank L. Quartier and M. Haddad for their valuable help. This work was finished during the stay of M.B.A. and A.B. at the Department of Mechanical Engineering of the MIT; M.B.A. and A.B. are grateful for the hospitality they received.

Correspondence and requests for materials should be addressed to A.B. (e-mail: arezki.boudaoud@lps.ens.fr).

Interconversion of single and double helices formed from synthetic molecular strands

Volker Berl*†, Ivan Huc‡*, Richard G. Khoury*, Michael J. Krische*§ & Jean-Marie Lehn*

* *Laboratoire de Chimie Supramoléculaire, ISIS, Université Louis Pasteur, 4 rue Blaise Pascal, F-67000 Strasbourg, France*
† *Forschungszentrum Karlsruhe GmbH, Institut für Nanotechnologie, Postfach 3640, D-76021 Karlsruhe, Germany*
‡ *Institut Européen de Chimie et Biologie, ENSCPB, Av. Pey Berland, F-33402 Talence Cedex, France*

Synthetic single-helical conformations are quite common, but the formation of double helices based on recognition between the two constituent strands is relatively rare. Known examples include duplex formation through base-pair-specific hydrogen bonding and stacking, as found in nucleic acids and their analogues, and polypeptides composed of amino acids with alternating L and D configurations[1,2]. Some synthetic polymers[3] and self-assembled fibres[4] have double-helical winding induced by van der Waals interactions. A third mode of non-covalent interaction, coordination of organic ligands to metal ions[5–7], can give rise to double, triple and quadruple helices, although in this case the assembly is driven by the coordination geometry of the metal and the structure of the ligands, rather than by direct inter-strand complementarity. Here we describe a family of oligomeric molecules with bent conformations, which exhibit dynamic exchange between single and double molecular helices in solution, through spiral sliding of the synthetic oligomer strands. The bent conformations leading to the helical shape of the molecules result from intramolecular hydrogen bonding within 2′-pyridyl-2-pyridinecarboxamide units[8–12], with extensive intermolecular

§ Present address: University of Texas at Austin, Department of Chemistry and Biochemistry, Austin, Texas 78712, USA.

aromatic stacking stabilizing the double-stranded helices that form through dimerization.

In the linear heptamers **1** to **3**, curvature of the strand should lead to a helical shape of the molecules (Fig. 1). Modelling studies suggest that coiling should extend to nearly one and a half turns. A 0.5-mM solution of **1** in $CDCl_3$ features a sharp ^{1}H NMR spectrum consistent with the presence of a single well defined species (Fig. 2a). The spectrum indicates that, on average, rings α, β and γ have the same environments as α′, β′ and γ′ respectively. Comparison of the spectrum of **1** to that of its shorter analogue **4** shows that a number of signals are substantially shifted upfield, suggesting intramolecular stacking interactions in **1**. For example, the terminal amide signals $C\underline{H}_2CON\underline{H}$ are found at 2.39 and 8.42 p.p.m. in **4**, and at 1.97 and 7.54 p.p.m. in **1**. Similarly, despite the almost symmetrical substitution of the β/β′ rings, one of the two aromatic protons of these rings is shifted upfield by 0.5 p.p.m. from the other (7.40 and 7.88 p.p.m. compared to 7.92 p.p.m. for protons of the β ring of **4**).

These features are consistent with the single-helix structure of **1** shown in Fig. 1. Indeed X-ray diffraction analysis indicated that **3**, a less soluble analogue of **1**, crystallized from DMSO/CH_3CN as a single-helix entity (Fig. 3a). Conformationally stabilized single molecular helices presenting up to four turns have been described recently[13–16].

Upon concentrating a solution of **1** in chloroform, a second set of signals appears on the ^{1}H NMR spectrum (Fig. 2b–d), indicating the presence of another species in slow exchange on the NMR timescale with the single-helix entity. Heating an 8.2-mM solution causes an increase of the proportion of the latter, up to over 98% at 55 °C, without any coalescence. The concentration and temperature dependence of the proportions between the two species suggests that the new signals correspond to an aggregate formed by two or more helical monomers. The exchange is clearly visible on the ^{1}H nuclear Overhauser enhancement spectroscopy (NOESY) spectra, which display cross-peaks between each signal of the monomer and each signal of the aggregate. Saturation transfer experiments yielded an exchange rate of 8.7 s^{-1} at 25 °C.

In the NMR spectra, the protons of the aggregate are overall more strongly shielded than the protons in monomeric species, suggesting that intermolecular π–π aromatic stacking is important in the aggregation process as expected for compounds containing several aromatic residues. However, simple stacking of independent helices should be fast on the NMR timescale and lead to a mixture of various oligomers instead of a well defined aggregate. Instead, aggregation apparently requires considerable conformational changes in the molecules. For these reasons, we proposed the formation of a double helix consisting of two intertwined monomeric strands, which would stack all along their length, so that association and dissociation would require winding and unwinding of the helical monomeric strands. A related process has been described for the formation of the double-helix gramicidin A dimer[2,17].

The proportions between the monomer and its aggregate at different concentrations (1–25 mM; see Fig. 2) are consistent with a dimerization constant K_{dim} of 25–30 l mol^{-1} in $CDCl_3$ at 25 °C. This value is strongly solvent dependent, being about 300, 22 and 95 l mol^{-1} for CD_2Cl_2, 1/9 $CDCl_3/CCl_4$, and 3/7 $CDCl_3/C_6D_{12}$ respectively. In all these solvents, however, increasing the concentration leads to broadening of the signals or precipitation, and not to analysable spectra of the aggregates.

The NMR spectra of the less soluble analogue **3** feature similar concentration dependence and slow exchange between monomeric and dimeric species (not shown). The proportions between these signals are in agreement with a dimerization constant of 110–120 l mol^{-1} in $CDCl_3$ at 25 °C. That these processes observed in solution do correspond to a double helix formation is supported by a crystal structure of the same compound **3**, which crystallized from nitrobenzene/heptane as a double helix (Fig. 3b).

As expected, the double-helix structure allows considerable overlap between the aromatic groups of each monomeric helical strand, with an average π–π stacking distance of 3.5 Å, corresponding to

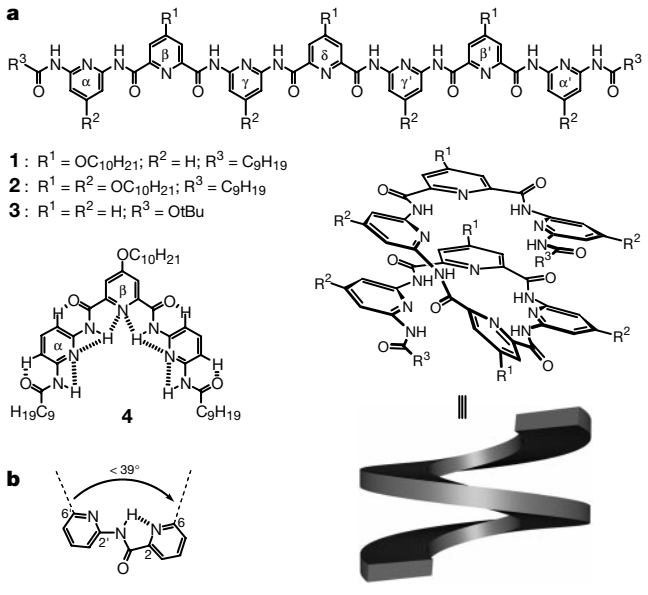

Figure 1 Structures and folding of oligopyridinecarboxamides. **a**, Formula of various oligomers and helical shape of a heptamer. These compounds were synthesized according to the scheme used for isophthalate analogues[20]. The decyloxy chains ensure the excellent solubility of **1** and **2** in chlorinated or aromatic solvents, and even in pure alkanes for **2**. **b**, Conformation of the 2′-pyridyl-2-pyridinecarboxamide motif. Conjugation of the aromatic rings with the amide moiety and intramolecular hydrogen bonding of the amide hydrogen to one pyridine ring is expected to stabilize one conformer in which substituents of the pyridine rings at the 6 and 6′ positions protrude on the same side of the molecule. Modelling studies indicate that these substituents define an angle reduced to 39°. In the solid state, this angle can be as low as 35° (ref. 8).

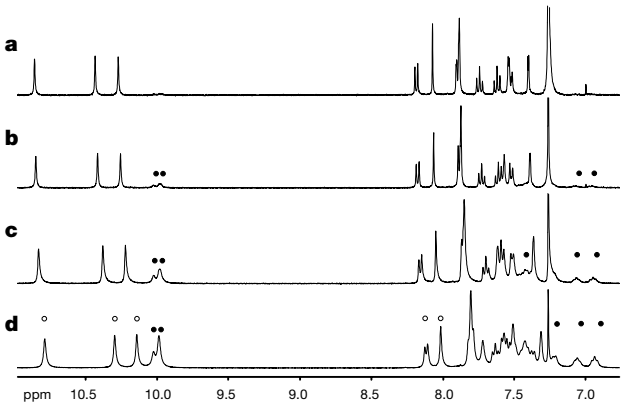

Figure 2 400-MHz ^{1}H spectra of $CDCl_3$ solutions of **1** at various concentrations at 25 °C. Some of the signals assigned to the monomer (unfilled circles), and to the dimer (filled circles) are labelled. **a**, 0.91 mM. The formation of intramolecular hydrogen bonds results in a strong deshielding of three of the four different amide protons (10.86, 10.43 and 10.27 p.p.m.), the terminal amide hydrogen being unable to undergo similar interactions; **b**, 2.7 mM; **c**, 8.2 mM; **d**, 24.5 mM. Nuclear Overhauser enhancement spectroscopy (NOESY) experiments confirm that the triplets observed at 7.06 and 6.94 p.p.m. correspond to the signals of the protons in position 4 of the α/α′ and γ/γ′ rings in the dimer.

van der Waals contact. The coulombic and van der Waals forces associated with aromatic stacking thus seem to promote interstrand attractive interactions. Most hydrogen bonds occur within the same strand and stabilize the helical shape of each monomer. Four direct interstrand NH-N hydrogen bonds occur at the ends of the duplex (3.19–3.32 Å and 3.21 Å), along with two bridging NH-O hydrogen bonds (3.01 and 3.09 Å) to a water molecule bound to the polar inner rim of the duplex. This structure contrasts with the structure of DNA, in which hydrogen bonding determines interstrand association, and stacking takes place mainly within each of the two strands.

The presence of bound water in the crystal lattice is consistent with previous crystallographic data[8,11], and with ^{1}H NMR solution studies of **1**, which feature a broad singlet between 3 and 5 p.p.m. This water molecule solvates the polar functions of **1**, and may contribute to the helical pre-organization. However, molecular modelling studies suggest that the water molecule is not necessary for helicity induction. Furthermore, the ratio of dimer versus monomer of **1** was found to increase significantly upon partial removal of water from the solvent ($CDCl_3$ or C_6D_6), whereas increasing the amounts of water led to the dissociation of the duplexes. This is possibly owing to the destabilization of the helical strand conformation as a result of water competing with intramolecular hydrogen bonding within **1**.

It should be emphasized that these solid-state characterizations of single and double molecular helices are from the same compound **3**, crystallized from different media. The single helix crystallized from a rather polar solvent mixture, whereas the double helix crystallized from a less polar solvent mixture. This is consistent with a polarity-dependent equilibrium and supports the idea that these helices are indeed the two equilibrating species observed by NMR and that their formation involves polar interactions.

Compound **2,** bearing four additional decyloxy chains, was expected to be more soluble in non-polar solvents. Its ^{1}H NMR spectra in $CDCl_3$ suggests that it also undergoes dynamic equilibrium between a single-helix monomer and a double-helix dimer (see Supplementary Information). In this case however, the dimer remains the major species at concentrations as low as 300 μM. Quantitative analysis of the NMR data led to a dimerization constant $K_{dim} = 6.5 \times 10^4\,l\,mol^{-1}$, which is three orders of magnitude larger than that of **1** in the same solvent. In toluene-D_8, CD_2Cl_2 and $C_2D_2Cl_4$, this value was found to be $5.5 \times 10^4\,l\,mol^{-1}$, $1.0 \times 10^5\,l\,mol^{-1}$, and $1.6 \times 10^5\,l\,mol^{-1}$ respectively. This marked effect may result from a larger number of interactions between the side chains as well as an increase in the interactions between

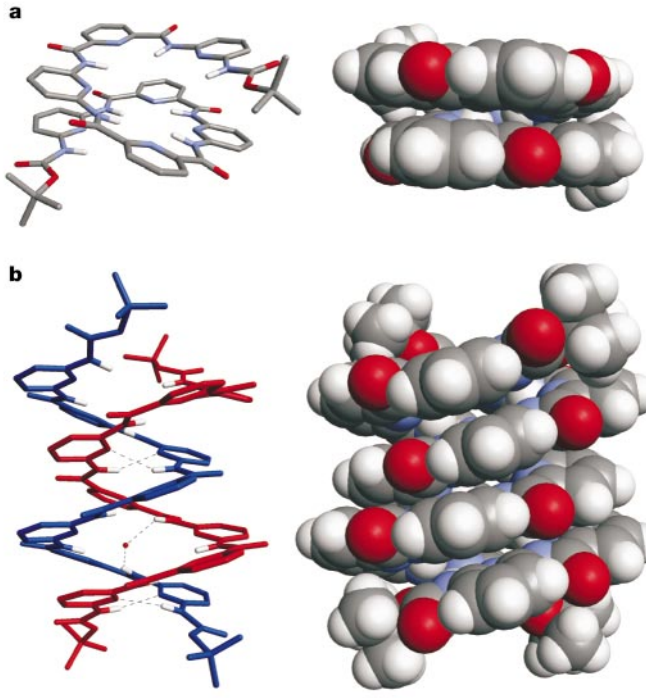

Figure 3 Crystal structures of the single helix and the double-helix dimer of **3**. The structures were determined by X-ray diffraction of two independent crystals. Solvent molecules included in the crystals and CH hydrogens in the stick representations are omitted for clarity. Carbon, grey; hydrogen, white; nitrogen, blue; oxygen, red. **a**, Single helix. Winding of the strand reaches one and a half turns, where one turn is generated by approximately five pyridine-amide units. Intramolecular π–π stacking is possible over half a helical turn, which is consistent with the upfield shift of some NMR signals observed in solution. **b**, Double-helix dimer. The stick representation with colour-coded strands shows interstrand hydrogen bonds (black dotted lines). Winding of the two strands results in a nearly two-turn duplex, with 16.7 Å in length, in which only four pyridine-amide units are needed per turn. Single/double helix interconversion corresponds to a spring-like compression/extension motion of each strand.

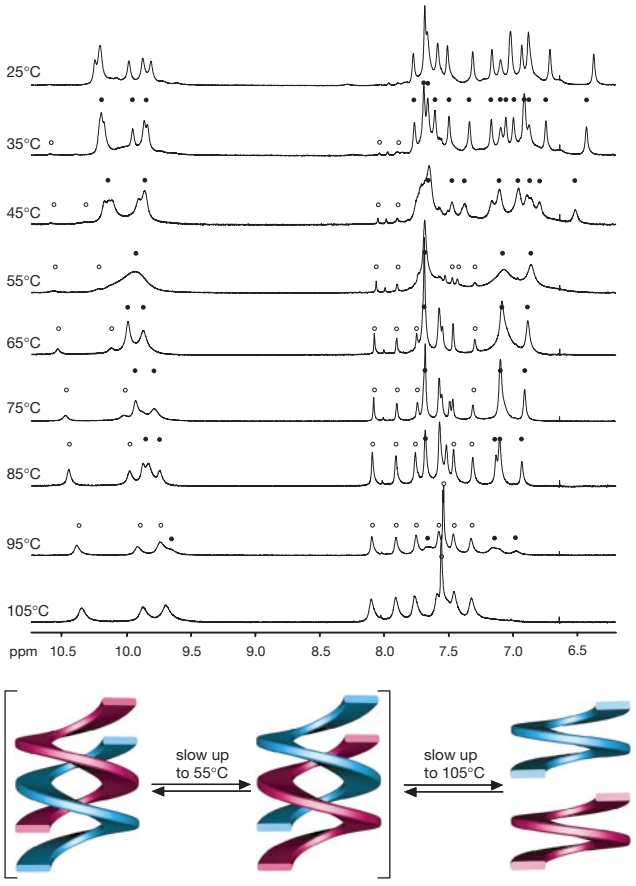

Figure 4 Formation and interconversion of double helices of **2**. Top, 400-MHz ^{1}H spectra of **2** (8.2 mM in $C_2D_2Cl_4$) at various temperatures. Some of the signals are assigned to the dimer (filled circles), to the monomer (unfilled circles), and to a minor impurity (asterisk). Bottom, schematic representations of the interconversion between two identical forms of dissymmetrical double helices by a sliding motion, and their dissociation into two single helices. In the dissymmetrical double-helical structures depicted, rings α and α′, β and β′, and γ and γ′ of an individual strand are situated in different local environments, and thus differ in their ^{1}H NMR signals. Their interconversion becomes rapid on the NMR timescale at 55 °C, and the signals associated with analogous protons in rings α and α′, β and β′, and γ and γ′ coalesce. The dissociation of the double helix into single helices is slow on the NMR timescale up to 105 °C.

aromatic rings due to the electron donor character of the decyloxy substituents in **2**.

We note two important differences between the proton signals of $(\mathbf{2})_2$ and $(\mathbf{1})_2$ in $CDCl_3$. The first refers to the broadness of the signals of $(\mathbf{2})_2$. This cannot be the result of exchange with monomer **2** whose signals would then broaden as well. More probably, it reflects slow conformational changes within $(\mathbf{2})_2$ or equilibration with other larger aggregates. The second difference is the non-equivalence of α/α', β/β', and γ/γ' rings in dimer $(\mathbf{2})_2$, which is apparent in $CDCl_3$ and clearly confirmed in $C_2D_2Cl_4$. In this latter solvent, the dimer signals are sharp at 25 °C and clearly indicate a dissymmetrical structure. In the hydrogen-bonded amide region (9.5-10.5 p.p.m.), six distinct signals of equal intensity can be counted instead of three for a symmetrical structure (see Supplementary Information). Between 6.5 and 8.5 p.p.m., the spectrum shows 16 partly overlapping singlets, corresponding to 14 different aromatic protons, and two different terminal amides NH. When we varied the concentration, the proportions between these signals remain unchanged. NOESY experiments show cross-peaks indicating slow exchange of half of the signals with the other half.

The evolution of the spectrum of **2** with temperature is shown in Fig. 4. At 25–35 °C the spectrum consists essentially of sharp signals of a dissymmetrical dimer. Above 45 °C, as the monomer proportion increases, its signals start to be clearly visible. Simultaneously, the dimer signals broaden substantially to coalesce at 55 °C. This spectrum is reminiscent of that observed in $CDCl_3$ at room temperature. Above 55 °C, the dimer signals sharpen again but their number is decreased. Although several signals overlap, the spectrum seems consistent with an averaged symmetrical structure such as the one observed for compound **1** (Fig. 2). At 95 °C, the monomer is by far the major species, and is still in slow exchange with the dimer. At 105 °C, the dimer peaks have disappeared, owing to their very low intensity, or because coalescence with the monomer has finally been reached.

In view of these data, the dimerization of compounds **1** and **2** appears to give rise to dissymmetrical double helices, so that the two ends of an individual strand are no longer equivalent (Fig. 4). Sliding of the monomers along one another in a spiralling motion and without dissociation allows each of the two ends of an individual strand to switch between states or local environments. Above a certain temperature, these equilibria become rapid on the NMR timescale. A related sliding process has been identified in the double-helix gramicidin A dimer[18,19]. We also note that such an interconversion would amount to the rotational translation of one strand with respect to the other, and thus it constitutes a molecular mechanical motion. □

Methods

Crystallographic data

Single crystals of **3** (single helix), $[C_{51}H_{47}H_{15}O_{10}{\cdot}2(C_2H_6SO){\cdot}2(H_2O){\cdot}1.5(C_2H_3N)]$, were grown from acetonitrile/dimethylsulphoxide. Crystals were placed in oil and a single colourless crystal of dimensions $0.25 \times 0.16 \times 0.15$ mm was selected, mounted on a glass fibre, and placed in a low-temperature N_2 stream. The unit cell was monoclinic with a space group of C2/c. Cell dimensions: $a = 33.952(7)$ Å, $b = 13.510(3)$ Å, $c = 27.970(6)$ Å, $\alpha = \gamma = 90°$, $\beta = 97.75(3)°$, $V = 12713(4)$ Å^3 and $Z = 8$ (FW is 1307.91, $\rho = 1.367$ g cm^{-3}). Reflections were collected from $1.0° \leq \theta \leq 27.6°$ for a total of 14,359 of which 7,699 were unique ($R_{int} = 0.089$) having $I > 4\sigma(I)$; number of parameters is 802. Final R factors were $R_1 = 0.117$ (based on observed data, w$R_2 = 0.254$ (based on all data), GOF = 1.067, maximal residual electron density is 0.933 e Å^{-3}. Single crystals of **3** (double helix), $[C_{51}H_{47}H_{15}O_{10}{\cdot}3(C_6H_5NO_2){\cdot}(H_2O)]$, were grown from heptane/nitrobenzene. The crystals were placed in oil and a single colourless crystal of dimensions $0.18 \times 0.15 \times 0.15$ mm was selected, mounted on a glass fibre, and placed in a low-temperature N_2 stream. The unit cell was triclinic with a space group of P$\bar{1}$. Cell dimensions: $a = 18.980(4)$ Å, $b = 19.230(4)$ Å, $c = 19.980(4)$ Å, $\alpha = 81.52(3)°$, $\beta = 75.11(3)°$, $\gamma = 81.59(3)°$, $V = 6926(2)$ Å^3 and $Z = 4$ (FW is 1417.38, $\rho = 1.350$ g cm^{-3}). Reflections were collected from $1.0° \leq \theta \leq 27.01°$ for a total of 30,136 of which 14,924 were unique ($R_{int} = 0.035$) having $I > 4\sigma(I)$; number of parameters = 1865. Final R factors were $R_1 = 0.099$ (based on observed data, w$R_2 = 0.214$ (based on all data), GOF is 1.005, maximal residual electron density is 0.600 e Å^{-3}.

X-ray diffraction data for **3** (single and double helix) was collected on a Nonius Kappa charge-coupled device (CCD) diffractometer with a graphite monochromatized MoKα radiation ($\lambda = 0.71071$ Å). φ scans, at 173 K. The structure solution of **3** (single and double helix) was determined using direct methods and refined (based on F^2 using all independent data) by full matrix least square methods (SHELXTL 97). Hydrogen atoms were included at calculated positions by using a riding model.

The crystal lattice of the single helix contains eight helical strands of **3** (four enantiomeric pairs) along with 16 molecules of DMSO, 12 molecules of acetonitrile and 16 molecules of water, out of which eight are located in the polar inner rim of the helices. The helical pitch of the helix is 3.5 Å and the pyridine–pyridine torsional angles are between 1.3° and 16.5° (average 10.1°).

The crystal lattice of the double-helix dimer contains four helical strands of **3** (two enantiomeric double-helix pairs), 12 molecules of nitrobenzene and two molecules of water bound to the polar inner rim of the double helix. Although the two strands of a duplex are crystallographically not equivalent, they are almost superimposable upon 180° rotation about the helical axis. The double-helix pitch is 7.2 Å and the pyridine torsional angles are opened up to between 17.9 and 34° (average 25.4°).

Received 11 April; accepted 17 August 2000.

1. Di Blasio, B., Benedetti, E., Pavone, V. & Pedone, C. Regularly alternating L,D-peptides. The double-stranded right-handed antiparallel β-helix in the structure of *t*-Boc-(L-Phe-D-Phe)$_4$-OMe. *Biopolymers* **28,** 203–214 (1989).
2. Langs, D. A. Three-dimensional structure at 0.86 Å of the uncomplexed form of the transmembrane ion channel peptide gramicidin A. *Science* **241,** 188–191 (1988).
3. Kusanagi, H. X-ray and energy calculation studies on the packing-mode of double-stranded helicies of isotactic poly(methyl methacrylate). *Polymer J.* **28,** 708–711 (1996).
4. Engelkamp, H., Middelbeek, S. & Nolte, R. J. M. Self-assembly of disk-shaped molecules to coil-coil aggregates with tunable helicity. *Science* **284,** 785–788 (1999).
5. Koert, M., Harding, M. & Lehn, J.-M. DNH Deoxyribonucleohelicates—self-assembly of oligonucleosidic double-helical metal complexes. *Nature* **346,** 339–342 (1990).
6. Hasenknopf, B., Lehn, J.-M., Kneisel, B. O., Baum, G. & Fenske, D. Self-assembly of a circular double helicate. *Angew. Chem. Int. Edn Engl.* **35,** 1838–1840 (1996).
7. Bell, T. W. & Jousselin, H. Self-assembly of a double-helical complex of sodium. *Nature* **367,** 441–444 (1994).
8. Redmore, S. M., Rickard, C. E. F., Webb, S. J. & Wright, L. J. Ruthenium complexes of a simple tridentate ligand bearing two 'distal' pyridine bases. *Inorg. Chem.* **36,** 4743–4748 (1997).
9. Hamuro, Y., Geib, S. J. & Hamilton, A. D. Novel folding patterns in a family of oligoanthranilamides: Non-peptide oligomers that form extended helical secondary structures. *J. Am. Chem. Soc.* **119,** 10587–10593 (1997).
10. Hamuro, Y., Geib, S. J. & Hamilton, A. D. Novel molecular scaffolds—formation of helical secondary structure in a family of oligoanthranilamides. *Angew. Chem. Int. Edn Engl.* **33,** 446–448 (1994).
11. Yu, Q. *et al.* Hydrogen bonded antiparallel beta-strand motifs promoted by 2,6-bis(carbamoylpeptide)pyridine. *Chem. Commun.* 1467–1468 (1999).
12. Mazik, M., Bläser, D. & Boese R. Hydrogen-bonding motifs in the crystals of secondary diamides with 2-amino-6-methyl and 2,6-diaminopyridine subunits. *Tetrahedron* **55,** 12771–12782 (1999).
13. Bassani, D., Lehn, J.-M., Baum, G. & Fenske, D. Designed self-generation of an extended helical structure from an achiral polyheterocyclic strand. *Angew. Chem. Int. Edn Engl.* **36,** 1845–1847 (1997).
14. Ohkita, M., Lehn, J.-M., Baum, G. & Fenske, D. Helicity coding: Programmed molecular self-organization of achiral nonbiological strands into multiturn helical superstructures: synthesis and characterization of alternating pyridine-pyrimidine oligomers. *Chem. Eur. J.* **5,** 3471–3481 (1999).
15. Cuccia, L. A., Lehn, J.-M., Homo, J.-C. & Schmutz, M. Encoded helical self-organization and self-assembly into helical fibers of an oligoheterocyclic pyridine-pyridazine molecular strand. *Angew. Chem. Int. Edn Engl.* **37,** 233–237 (2000).
16. Nelson, J. C., Saven, J. G., Moore, J. S. & Wolynes, P. G. Solvophobically driven folding of nonbiological oligomers. *Science* **277,** 1793–1796 (1997).
17. Veatch, W. R. & Blout, E. R. The aggregation of gramicidin A in solution. *Biochemistry* **13,** 5257–5264 (1974).
18. Sychev, S. V., Barsukov, L. I. & Ivanov, V. T. The double ππ5.6 helix of gramicidin A predominates in unsaturated lipid membranes. *Eur. Biophys. J.* **22,** 279–288 (1993).
19. Barsukov, I. L., Arseniev, A. S. & Bystrov, V. F. Spatial structures of gramicidin A in organic solvents. ^{1}H-NMR analysis of four species in ethanol. *Bioorg. Khim.* **13,** 1501–1522 (1987).
20. Berl, V., Krische, M. J., Huc, I., Lehn, J.-M. & Schmutz, M. Template-induced and molecular recognition-directed hierarchical generation of supramolecular assemblies from molecular strands. *Chem. Eur. J.* **6,** 1938–1946 (2000).

Supplementary information is available on *Nature*'s World-Wide Web site (http://www.nature.com) or as paper copy from the London editorial office of *Nature*.

Acknowledgements

We thank J. Fischer and A. DeCian for the use of the X-ray crystallographic facilities at ULP, Strasbourg. This work was supported by the CNRS, by a predoctoral fellowship (V.B.) from the Forschungszentrum Karlsruhe GmbH, Germany, and by a NSF-NATO postdoctoral fellowship (R.G.K.).

Correspondence and requests for materials should be addressed to I. H. (e-mail: ivan.huc@iecb-polytechnique.u-bordeaux.fr) or J.-M. L. (e-mail: lehn@chimie.u-strasbg.fr). Crystallographic data for **3** (excluding structure factors) have been deposited with the *Cambridge Crystallographic Data Centre* as supplementary publication no. CCDC-142810 (**3**, single helix) and CCDC-142811 (**3**, double helix). Copies of the data can be obtained free of charge on application to CCDC, 12 Union Road, Cambridge CB2 1EZ, UK.